ADVANCED THEORY AND SIMULATIONS
www.advtheorysimul.com

Tunable Electronic Properties of Novel 2D Janus $MSiGeN_4$ (M = Ti, Zr, Hf) Monolayers by Strain and External Electric Field

*Vo T.T. Vi, Tran P.T. Linh, Cuong Q. Nguyen, and Nguyen N. Hieu**

Since the recent successful experimental synthesis of $MoSi_2N_4$ [Science, 369 (2020), 670], the "MA_2Z_4 family" has been of particular interest to the scientists in the field of materials science due to its outstanding physical properties. In this paper, the first-principles calculations are performed to study the structural, elastic, and electronic properties of novel two-dimensional (2D) Janus $MSiGeN_4$ monolayers (M = Ti, Zr, Hf). The calculations of phonon spectra indicate that monolayers $MSiGeN_4$ are dynamically stable and can be experimentally synthesized. The obtained Young's modulus and Poisson's ratio of the Janus structures $MSiGeN_4$ are much larger than that of other binary 2D materials and meet the mechanical stability criteria suggested by Born and Huang. In the calculations using either PBE or HSE06 functionals, the Janus $MSiGeN_4$ structures exhibit indirect semiconductor characteristics with larger band gaps than that of similar septuple-atomic-layer materials, such as $MoSiGeN_4$ and $WSiGeN_4$. In addition, the influences of biaxial strain and external electric field on the electronic structure of $MSiGeN_4$ are investigated. It is found that the biaxial strain tunes the electronic characteristics more significantly than the external electric field. The obtained results can provide insights into novel Janus monolayers with potential applications in electronic devices.

1. Introduction

In the last two decades, two-dimensional (2D) materials have become one of the most interesting objects due to their distinct properties compared to bulk structures. Some typical materials can be mentioned as graphene,[1–4] transition metal dichalcogenides,[5–8] post-transition metal monochalcogenides,[9–11] etc. with many unique physical properties as well as potential applications in nanoelectronic devices. The graphene family is constantly expanding with many compounds discovered and successfully synthesized. In particularity, the successful synthesis of the 2D Janus asymmetric material MoSSe[12,13] recently opened a bright future for studies of 2D materials.[14] Many subsequent studies have focused on the 2D Janus structures and the heterostructures formed from these new materials.[15–20] With their vertical broken mirror symmetry structure, they have had many extraordinary physical properties with potential applications in the fields of materials science, energy conversion, and spintronics.[21–23]

Recently, a new 2D structure $MoSi_2N_4$ has been successfully fabricated by chemical vapor deposition.[24] Monolayer $MoSi_2N_4$ has been shown to have an energy gap value of 1.94 eV and it can serve as a photocatalyst in photocatalytic applications. $MoSi_2N_4$ monolayer possesses very high electron mobility up to 270 $cm^2 V^{-1} s^{-1}$.[24] The electronic properties of 2D materials depend strongly on their structural geometry and particularly on the number of atomic layers in the compounds. Wang et al.[25] have proposed an efficient strategy to design the septuple-atomic-layer systems MA_2Z_4 (A = transition-metal elements; A = Si, Ge; and Z = N, P, As), which contain 72 structures with thermal and dynamic stability. XY_2Z_4 compounds show extremely diverse and unusual electronic features, they can be semiconductors, non-magnetic metals, ferromagnetic semiconductors, or topological insulators.[25] Also, van der Waals heterostructures based on $MoSi_2N_4$ such as $C_3N_4/MoSi_2N_4$[26] and $MoSH/MoSi_2N_4$[27] have been also designed and investigated theoretically. Besides, $MoSi_2N_4$-based Janus structures $MoSiGeN_4$ and $WSiGeN_4$ have been proposed recently.[28] It is found that both $MoSiGeN_4$ and $WSiGeN_4$ monolayers are indirect semiconductors with appropriate band alignment for photocatalytic performance.[28]

V. T. Vi
Faculty of Basic Sciences
University of Medicine and Pharmacy
Hue University
Hue 530000, Viet Nam
T. P. Linh
Faculty of Physics
Hanoi National University of Education
Ha Noi 100000, Viet Nam
C. Q. Nguyen, N. N. Hieu
Institute of Research and Development
Duy Tan University
Da Nang 550000, Viet Nam
E-mail: hieunn@duytan.edu.vn
C. Q. Nguyen, N. N. Hieu
Faculty of Natural Sciences
Duy Tan University
Da Nang 550000, Viet Nam

The ORCID identification number(s) for the author(s) of this article can be found under https://doi.org/10.1002/adts.202200499

DOI: 10.1002/adts.202200499

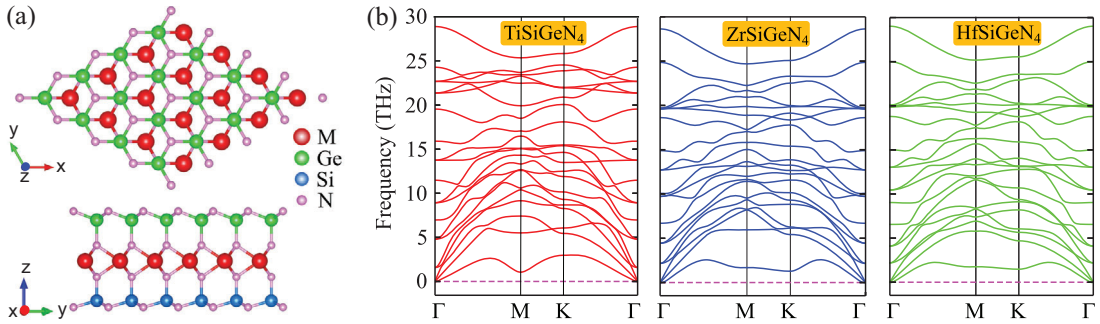

Figure 1. a) Top view and b) side view of 2D relaxed Janus $MSiGeN_4$ (M = Ti, Zr, Hf). c) Phonon spectra of 2D Janus $MSiGeN_4$ (M = Ti, Zr, Hf).

Promoted by the discovery of septuple-atomic-layer configurations and Janus structures based on these materials, we propose novel Janus structures $MSiGeN_4$ (M = Ti, Zr, Hf). We focus on the structural, elastic, and electronic properties of $MSiGeN_4$ monolayers based on the investigation by first-principles calculations. We also study the effects of external conditions, such as mechanical strains and external fields, on the electronic states of $MSiGeN_4$ monolayers. The obtained results of the paper are presented as follows. First, we report structural parameters and analyze phonon spectra of three Janus configurations $MSiGeN_4$ (M = Hf, Ti, Zr). Next, we calculate the elastic constants and cohesive energy to check the structural stability of the studied systems. In addition, the electronic band structure, band gaps, projected band structures, and work functions of all systems are studied. Finally, we examine the influences of biaxial strains and external electric fields on the electronic properties of these Janus monolayers.

2. Computational Details

In this study, the geometric optimization and electronic properties of the $MSiGeN_4$ (M = Ti, Zr, Hf) structures are calculated by first-principles calculations as carried out in the Quantum Espresso simulation packages.[29] The generalized gradient approximation (GGA) of Perdew–Burke–Ernzerhof (PBE)[30] is used to calculate the electronic exchange and correlation. The Heyd–Scuseria–Ernzerhof (HSE06) hybrid functional[31] is also used to get a more accurate value of the band gap. To consider the weak van der Waals (vdW) interactions between interlayers, the semiempirical DFT-D2 method[32] is adopted. The cut-off energy of 520 eV is selected for the plane-wave expansion and Monkhorst–Pack grids of 15 × 15 × 1 *k*-point mesh are chosen for the Brillouin zone. The convergences of energy and forces are set to be 10^{-6} eV and 10^{-3} eV $Å^{-1}$, respectively. A vacuum space of 25 Å along the *z*-direction is used to exclude the interactions between adjacent monolayers. Phonon spectra of the studied monolayers are calculated using density functional perturbation theory.[33]

3. Results and Discussion

3.1. Atomic Structures and Structural Stability

The top and side views of optimized atomic structures of 2D Janus $MSiGeN_4$ (M = Ti, Zr, Hf) monolayers are illustrated in **Figure 1**. The 2D Janus $MSiGeN_4$ monolayers could be considered as Si–N and Ge–N bilayers sandwiched by M–N_2 monolayers. These three structures can be constructed from MSi_2N_4 by replacing one layer of Si atoms by a single layer of Ge atoms. Monolayer $MSiGeN_4$ has a hexagonal structure as shown in Figure 1a. Its atomic structure is arranged in stacking order layers N–Si–N–M–N–Ge–N as shown in Figure 1b. Because of the lack of mirror symmetry, the symmetry of Janus $MSiGeN_4$ (M = Ti, Zr, Hf) monolayers (#156) is lower than symmetry of MGe_2N_4 or MSi_2N_4 (#187). The reduction of symmetry, however, results in many unique properties of these materials. The obtained results show that the optimized lattice constants of Janus $TiSiGeN_4$, $ZrSiGeN_4$, and $HfSiGeN_4$ are 2.97, 3.07, and 3.06 Å, respectively. Besides, the monolayer thickness of the investigated structures is carried out and presented in **Table 1**. Among these three structures, $TiSiGeN_4$ possesses the lowest lattice constant and thickness, while those values are nearly equal for $ZrSiGeN_4$ and $HfSiGeN_4$. Note that the lattice constant of $ZrSiGeN_4$ (3.07 Å) is slightly larger than that of $HfSiGeN_4$ (3.06 Å) despite Zr having a smaller atomic radius than Hf element. This phenomenon has also been observed in similar Janus structures (ZrSSe and HfSSe).[34] The lowest ionic radius of Ti^{4+} and the similarity in ionic radii of Zr^{4+} and Hf^{4+} are attributed to that discrepancies.

Table 1. The lattice constant *a*, thickness *h*, cohesive energy E_c elastic constants C_{11}, C_{12}, and C_{66}, Young's modulus Y_{2D} and Poisson's ratio $\mathcal{P}$ of 2D Janus $MSiGeN_4$ (M = Ti, Zr, Hf) monolayers.

	a [Å]	*h* [Å]	E_c [eV atom^{-1}]	C_{11} [N m^{-1}]	C_{12} [N m^{-1}]	C_{66} [N m^{-1}]	Y_{2D} [N m^{-1}]	$\mathcal{P}$
$TiSiGeN_4$	2.97	7.10	−8.00	450.79	142.26	154.27	405.90	0.32
$ZrSiGeN_4$	3.07	7.20	−8.05	410.21	137.46	136.38	364.15	0.34
$HfSiGeN_4$	3.06	7.18	−8.11	430.16	142.84	143.66	382.73	0.33

To examine the structural stability of the proposed Janus structures, we first test the chemical bond strength based on the evaluation of cohesive energy. The cohesive energy E_c of $MSiGeN_4$ monolayer can be calculated as follows

$$E_c = \frac{E_{tot} - (N_M E_M + N_{Si} E_{Si} + N_{Ge} E_{Ge} + N_N E_N)}{N_M + N_{Ge} + N_{Si} + N_N} \quad (1)$$

where E_{tot} is the total energy of $MSiGeN_4$ sheet; E_ζ and N_ζ are the enegy of single-atom ζ and number of the ζ atoms in the unitcell (ζ = M, Ge, Si, N), respectively.

The obtained results, as listed in Table 1, indicate that all three structures of $MSiGeN_4$ have negative cohesive energies. The negative cohesive energy calculated by Equation (1) implies that $MSiGeN_4$ monolayers are all energetically favorable. With high cohesive energy, about −8 eV atom^{-1}, the chemical bonds in the Janus $MSiGeN_4$ monolayers are stronger than those in many other existing 2D layered structures.

Next, we study the vibrational spectrum to evaluate the stability of Janus $MSiGeN_4$. The phonon dispersions calculations are calculated and described in Figure 1b. A material is recognized to be dynamically stable if its phonon spectrum contains positive frequencies throughout the Brillouin zone. As it is clear from this figure, phonon spectra of all these Janus materials consist of twenty-one modes, of which three are acoustic and eighteen are optical. At Γ point, there are six double-degenerate and six non-degenerate optical branches. Notably, the negative modes are absent in the Brillouin zone, proving that all three Janus $MSiGeN_4$ are dynamically stable and can be synthesized experimentally.

To explore the mechanical stability of Janus structures, we calculate and analyze the elastic constants according to Born–Huang's criteria for mechanical stability. In principle, there are four independent elastic constants to be tested for 2D materials, namely C_{11}, C_{22}, C_{12}, and C_{66} (in Voigt notation). As shown in Figure 1a, three Janus $MSiGeN_4$ have hexagonal structures resulting in $C_{11} = C_{22}$. Thus, we only need to calculate three elastic constants, C_{11}, C_{12}, and C_{66}, in which C_{66} is calculated via C_{11} and C_{12} according to the equation $C_{66} = (C_{11} - C_{12})/2$. To get the elastic constants C_{ij} we used a strain range from −0.015 to 0.015 in increments of 0.005 along the x- and y-axes. We then consider the energy change of Janus with respect to small strains along the two axes mentioned above. The elastic constants C_{11} and C_{12} are found by polynomial fitting the strain-dependence of energy values.[35] Table 1 presents the calculated results of the elastic constants of all Janus structures. They have elastic constants C_{11} ranging from 410.21 to 450.79 N m^{-1} and C_{12} ranging from 137.46 to 142.84 N m^{-1}. According to Born–Huang's criteria for mechanical stability, a material is considered to be mechanically stable if $C_{11} > 0$ and $C_{11}^2 - C_{12}^2 > 0$.[36] It is found that the elastic constants of all studied Janus structures $MSiGeN_4$ meet Born–Huang's criteria, demonstrating their structure to be mechanical stability.

Besides the elastic constants, we also consider Young's modulus and Poisson's ratio of 2D $MSiGeN_4$ monolayers. These parameters can be calculated based on the constants C_{ij}. The direction-dependent 2D Young's modulus $Y_{2D}(\varphi)$ and Poisson's ratio $\mathcal{P}(\varphi)$ can be written by[37,38]

$$Y_{2D}(\varphi) = \frac{C_{11}C_{22} - C_{12}^2}{C_{11}\sin^4\varphi + C_{22}\cos^4\varphi - (2C_{12} - \Pi)\sin^2\varphi\cos^2\varphi} \quad (2)$$

$$\mathcal{P}(\varphi) = \frac{C_{12}(\sin^4\varphi + \cos^4\varphi) - (C_{11} + C_{22} - \Pi)\sin^2\varphi\cos^2\varphi}{C_{11}\sin^4\varphi + C_{22}\cos^4\varphi - (2C_{12} - \Pi)\sin^2\varphi\cos^2\varphi} \quad (3)$$

where $\Pi = (C_{11}C_{22} - C_{12}^2)/C_{66}$ and φ is the angle relative to the armchair axis.

The polar diagrams of $Y_{2D}(\varphi)$ and $\mathcal{P}(\varphi)$ of 2D Janus $MSiGeN_4$ monolayers are shown **Figure 2**. It is found that the graphs $Y_{2D}(\varphi)$ and $\mathcal{P}(\varphi)$ are perfectly circles. This suggests that Janus $MSiGeN_4$ monolayers have isotropic elastic properties. This is due to the isotropic structure of these monolayers as depicted in Figure 1 a. The calculated results for Y_{2D} and $\mathcal{P}$ are presented in Table 1. It is calculated that the Janus $MSiGeN_4$ has Young's modulus ranging from 364.15 to 405.90 N m^{-1}. The change in Y_{2D} values of $MSiGeN_4$ monolayers does not follow the trend that Young's modulus decreases as the atomic radius of M varies from Ti to Hf. This may be due to the atomic structure, especially their lattice constant, as described above. The Y_{2D} values of $MSiGeN_4$ monolayers are much higher than that of other 2D nanostructures, such as monolayers SnSSe,[39] GaInXO (X = S, Se, Te),[17] even larger than that of graphene.[40] The Poisson's ratio of three Janus structures is almost the same, in the range from 0.32 to 0.34. These results are much larger than the Poisson's ratio of graphene[40] or C_2F_4.[41]

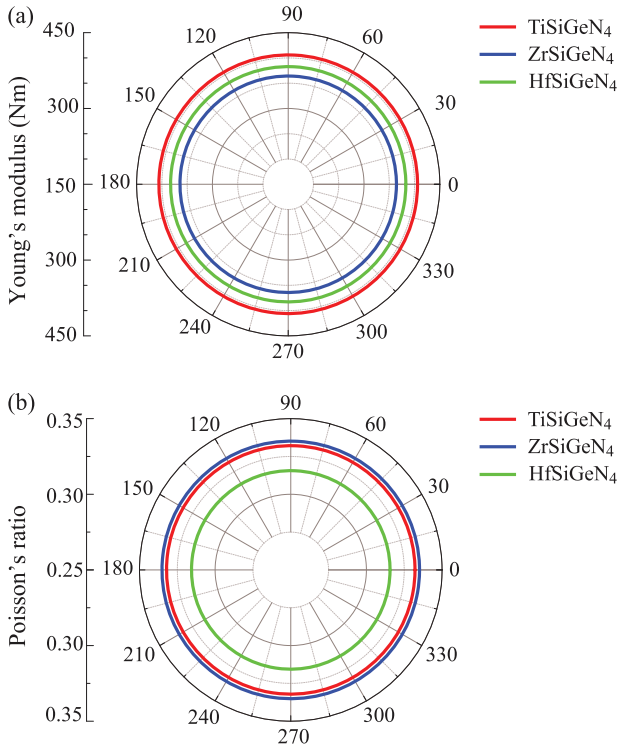

Figure 2. a) Young's modulus and b) Poisson's ratio of 2D Janus $MSiGeN_4$ (M = Ti, Zr, Hf).

3.2. Electronic Properties

Electronic properties and energy gap are the first characteristics that need to be examined if the material is to be applied to devices, especially electronic devices. Here, we calculate the electronic structures of the Janus $MSiGeN_4$ monolayers by using the different exchange-correlation functionals. **Figure 3** shows the band structures of the Janus $MSiGeN_4$ monolayers calculated by using the PBE functional. From Figure 3 we observe that three Janus $MSiGeN_4$ are indirect-gap semiconductors. The CBM lies on the KΓ line for all three monolayers, whereas the VBM lies on the ΓM and MK path for $TiSiGeN_4$ and $ZrSiGeN_4$, $HfSiGeN_4$ monolayers, respectively. At the PBE level, the obtained band gap values

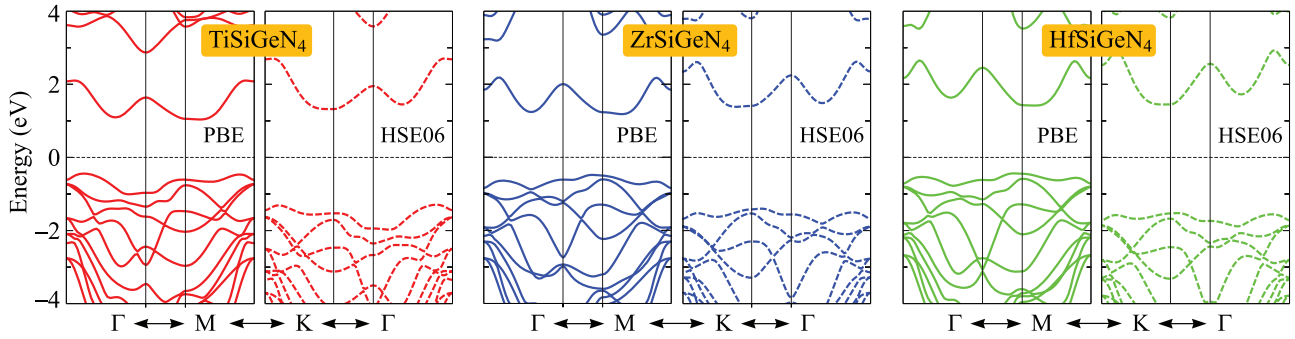

Figure 3. Electronic band structure of 2D Janus $MSiGeN_4$ (M = Ti, Zr, Hf) by PBE and HSE06 methods.

Table 2. Calculated band gap E_g by PBE and HSE06 functionals, and work functions on NSi side Φ_1 and NGe side Φ_2 of 2D Janus $MSiGeN_4$ (M = Ti, Zr, Hf).

	E_g^{PBE} [eV]	E_g^{HSE06} [eV]	$\Delta\Phi$ [eV]	Φ_1 [eV]	Φ_2 [eV]
$TiSiGeN_4$	1.48	2.62	0.37	6.80	7.16
$ZrSiGeN_4$	1.66	2.79	0.12	6.83	6.95
$HfSiGeN_4$	1.86	2.97	0.19	6.88	7.07

for $TiSiGeN_4$, $ZrSiGeN_4$, $HfSiGeN_4$ are 1.48, 1.66, and 1.86 eV, respectively. It can be seen that the band gaps of Janus $MSiGeN_4$ increase as M changes from Ti to Hf. However, in the DFT simulations, the PBE approach underestimates the energy gap accuracy for the semiconductors and insulators. One can treat this problem by using the GW approach or hybrid functional. Hence, in this paper, in addition to the PBE method, the HSE06 method is used to improve the band structure of all studied Janus. Our obtained results indicate that the Janus $MSiGeN_4$ monolayers also exhibit indirect semiconductor characteristics by the HSE06 method, which is the same as the PBE method. The evaluated band diagrams by the PBE and HSE06 methods are similar in profile as shown in Figure 3. However, the HSE06 approach gives a much larger energy gaps value than the PBE functional. **Table 2** shows the significant difference in energy gaps calculated by the two methods mentioned above. The band gap values calculated by the HSSE06 method also increased with the same trend as that calculated within the PBE. The band gaps of our three proposed Janus are larger than that of similar Janus materials, such as $MoSiGeN_4$ and $WSiGeN_4$.[28]

To get insights into the nature of the formation of electronic bands, we have also calculated weighted band structures and analyzed in detail the contribution of constituents to the electronic energy band structure, especially their contribution to CBM and VBM, of the Janus $MSiGeN_4$ monolayers. The weighted band structure of 2D Janus $MSiGeN_4$ is shown in **Figure 4**. As it is clear from this figure, all three Janus structures have similar weighted band structures. The CBM of Janus is contributed significantly by the hybridization of the M and Ge atoms. However, the main contribution to VBM is derived from the hybridization between N and Ge atoms.

In addition, we also calculated the work function for 2D Janus $MSiGeN_4$. This is one of the important electronic properties of materials, based on which we know the ability of electrons to escape from the surfaces of materials. The work function depends on the vacuum level $\Phi = E_{vac}$ and the Fermi level E_F according to the expression $\Phi = E_{vac} - E_F$. In the Janus structures, a built-in electric field exists due to their vertically asymmetrical structure.[42] The difference in electronegativity between different atomic layers in the *z*-axis causes the electric field to appear in

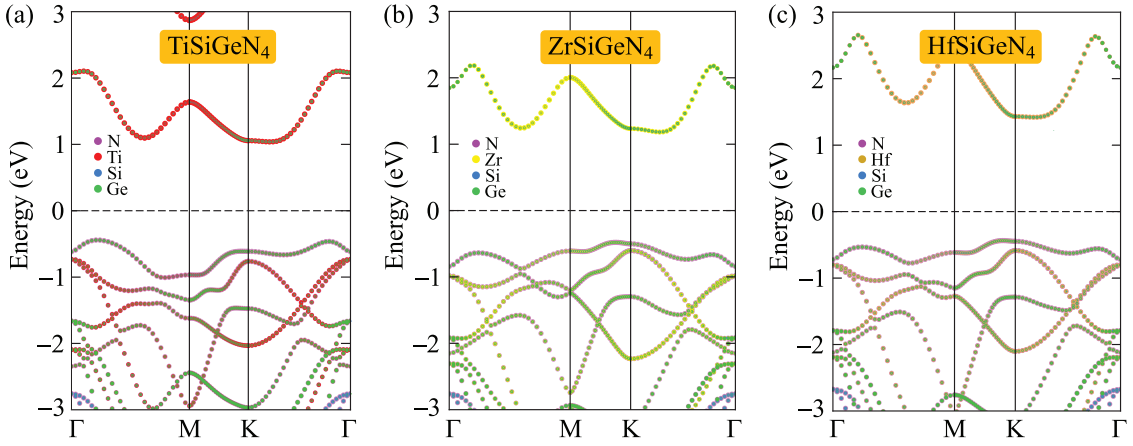

Figure 4. Projected band structure of 2D Janus a) $TiSiGeN_4$, b) $ZrSiGeN_4$ and c) $HfSiGeN_4$.

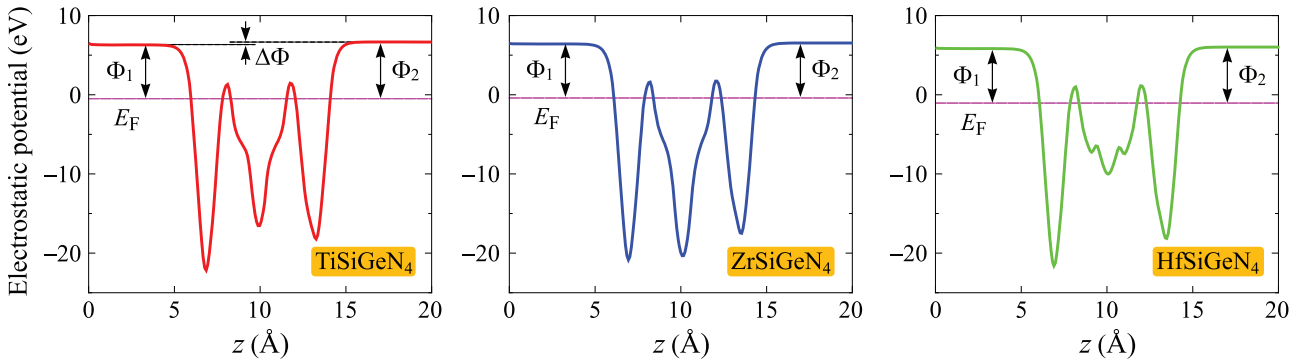

Figure 5. Electrostatic potential of 2D Janus a) $TiSiGeN_4$, b) $ZrSiGeN_4$ and c) $HfSiGeN_4$.

the Janus structure. For these structures, the dipole corrections should be included. We can use the dipole corrections to cancel artificial fields generated by periodic boundary conditions.[43] Our calculations for the electrostatic potentials (**Figure 5**) of the Janus $MSiGeN_4$ monolayers indicate that the difference in the vacuum level between the two surfaces Φ_{vac} is small as listed in Table 2. This is due to the small difference in electronegativity between Si and Ge elements on the two sides of the Janus structures. Calculated work functions on the NSi-side Φ_1 and the NGe-side Φ_2 are also listed in Table 2.

3.3. Electronic Properties of $MSiGeN_4$ under Biaxial Strain and External Electric Field

Many previous reports have demonstrated that the electronic structures of 2D layered nanostructures are easily modulated under the influence of external conditions. Specifically, the strain caused a direct–indirect semiconductor transition and vice versa, or a semiconductor–metal transition in 2D monolayers and 2D Janus structures.[15,16,44–46] Besides, the external electric field also causes the same changes as in the strain case.[16,46,47] Following

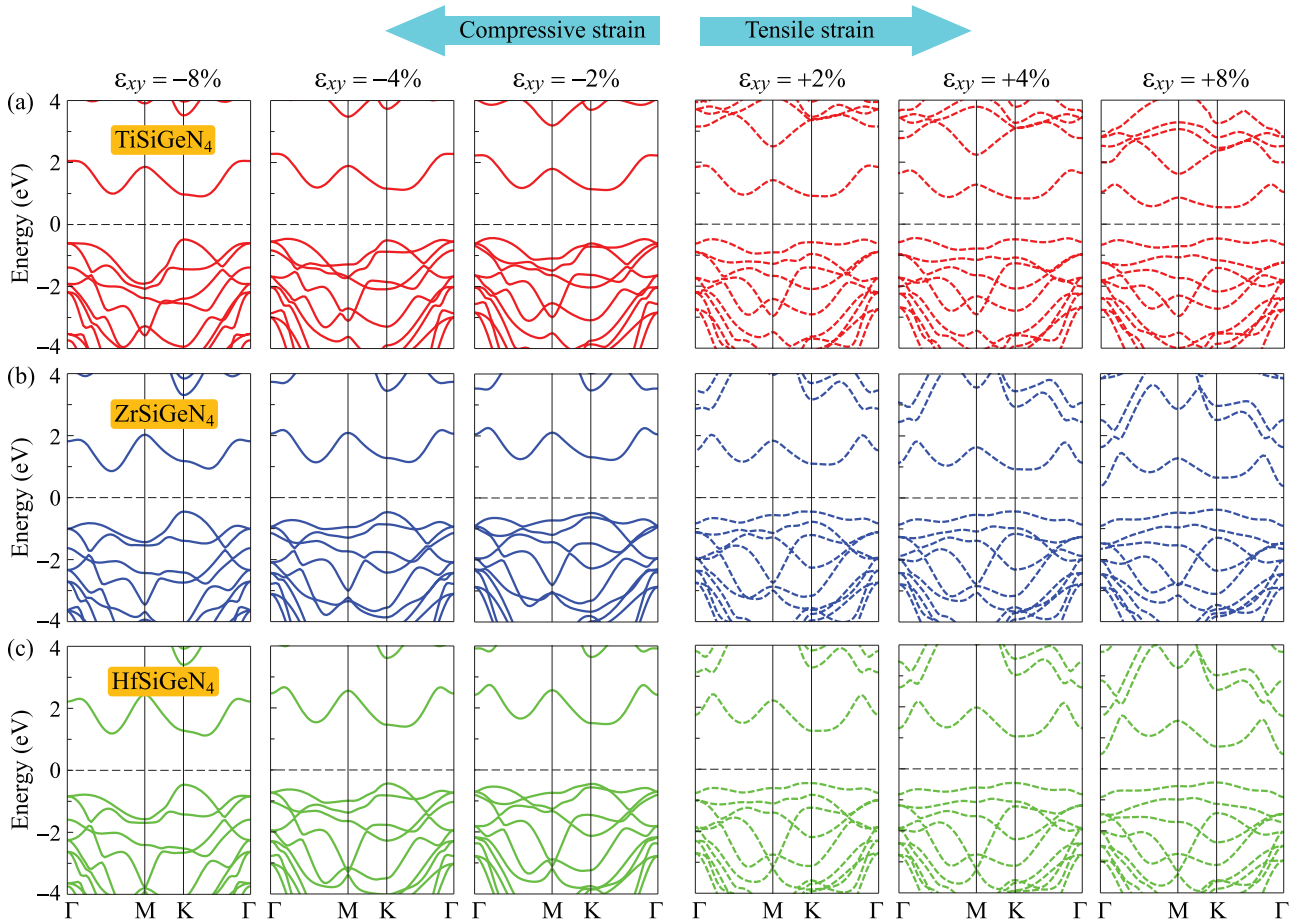

Figure 6. Electronic band structure under biaxial strain of 2D Janus a) $TiSiGeN_4$, b) $ZrSiGeN_4$, and c) $HfSiGeN_4$ monolayers.

that trend, we investigated the influence of biaxial strain and external electric field on the electronic features of three 2D Janus $MSiGeN_4$.

We first consider how the electronic properties of 2D Janus $MSiGeN_4$ depend on the biaxial strain. The biaxial strain is defined as $\varepsilon_{xy} = (a - a_0)/a_0$, where a_0 and a are the undistorted and distorted lattice constants of the Janus structures, respectively. In this work, we investigate the strain range from −10% to +10%, in which the positive sign corresponds to tensile strain and the negative sign corresponds to compressive strain.

The dependence of electronic band structures of the Janus structures on strain is clarified in **Figure 6**. It can be found that strain had a great influence on their electronic band structure. Before evaluating the detailed effect of strain on each Janus structure, we give a general picture of change for all three Janus. When the strain is introduced, the bond lengths will be changed. This can cause the coupling strength between atomic orbitals to be weakened or strengthened. As a result, the electronic structure will be changed significantly. As illustrated in Figure 6, the deformation shifted the positions of the CBM and the VBM between the high symmetric points in the Brillouin zone. At the same time, with increasing strain intensity, both the CBM and VBM approach the Fermi level. The energy band structure changes more significantly in the case of a tensile strain than in the case of compressive strain. Although the positions of the CBM and VBM are changed, all studied Janus retain the indirect semiconductor characteristics. As the CBM and VBM move closer to the Fermi level, the band gaps of these Janus decrease as the strain degree increases.

We further analyze in detail the change of electronic band structure in each 2D Janus $MSiGeN_4$ monolayer under biaxial strain conditions. In Janus $TiSiGeN_4$, the VBM shifted from the ΓM-path to the K point when it was subjected to −6%, +6% strain, whereas CBM does not change position under the strain (remains on the KΓ line). Therefore, no phase transition was observed in Janus $TiSiGeN_4$. For the Janus $ZrSiGeN_4$, the VBM position changed immediately when the strain is applied. VBM lying on the MK line shifted to K point at 2% strain intensity. Meanwhile, the CBM on the KΓ path shifted to the Γ point under 6% tensile strain and the ΓM line under −6% compressive case. Indirect semiconductor characteristics remain unchanged. In terms of Janus $HfSiGeN_4$, the VBM located on the MK line moves to K point when tensile strain 2% is introduced, and CBM moves from KΓ path to Γ under strain magnitude +8%. For compressive conditions, CBM remains on the KΓ line, while VBM has shifted to K point as soon as compressive strain is only −2%. As a result, the phase transition was not found in Janus $HfSiGeN_4$.

In addition to using strain, the external electric field is one of the common methods to control the electronic structure of a material. Herein, we use an external electric field placed perpendicular to the 2D surface of Janus. The intensity of the electric field varies from −5 to +5 V nm^{-1}. The electric field is positive if its direction is along the positive z-axis and negative if its direction is opposite to the z-axis direction. It is found that the band structure of all three Janus depends very weakly on the electric field (not shown). The VBM and CBM remain in the same position without an external electric field. The band gaps of these monolayers do not change significantly when an external electric field is applied.

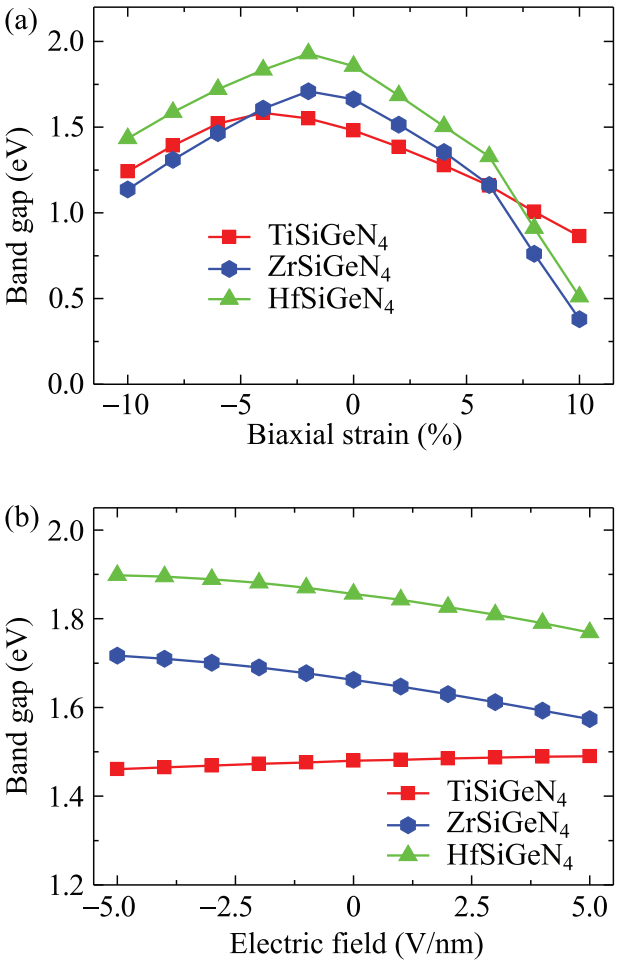

Figure 7. Band gaps under a) strain and b) external electric field of 2D Janus $MSiGeN_4$.

The evolution of band gaps of all Janus $MSiGeN_4$ structures with different biaxial strain and external electric field intensity is illustrated in **Figure 7**. Figure 7a indicates that the trend of band gap change with the applied biaxial strain of all monolayers is quite similar. In the tensile case, the energy gap is reduced rapidly. Meanwhile, compressive strain increases the band gap slightly and then reduces the band gap if strain magnitude is further increased. The strain has a strong influence on the energy gaps of the studied structures. In the whole strain range from −10% to 10%, the difference between the maximum and minimum values of the band gaps in $HfSiGeN_4$ is the largest (1.42 eV), then in $ZrSiGeN_4$ (1.33 eV) and finally in $TiSiGeN_4$ (0.72 eV). The energy gap dependence on the strain of Janus $MSiGeN_4$ follows the same trend as that of Janus M_2XY monolayers.[15,16] The technique of altering electronic properties by using strain could lead to potential applications of our studied Janus structures in electromechanical devices. Unlike the strain case, the influence of the electric field on band gap values is quite weak. From Figure 7b it is found that the band gap is approximately linearly dependent on the electric field. However, the energy gap values are almost unchanged, especially in Janus $TiSiGeN_4$ monolayer, the E_g difference under an external electric field ranging from −5 to

5 V nm^{-1} is only 0.03 eV. The energy disparity in the other two Janus is also not significant, 0.15 and 0.13 eV in $ZrSiGeN_4$ and $HfSiGeN_4$, respectively. The dependence of the electronic properties weakly on the external electric field has also been observed in the previous works.[15,16,46]

4. Conclusions

In conclusion, we performed a first-principles study in order to investigate the structural, elastic properties, and electronic characteristics of three 2D Janus monolayers $MSiGeN_4$ (M = Ti, Zr, Hf) at equilibrium state as well as under biaxial strains and electric fields. Our results reveal that 2D Janus $MSiGeN_4$ monolayers have dynamically stable structures, high mechanical strength, and isotropic elastic properties. The Janus monolayers $MSiGeN_4$ have a high Young's modulus and Poisson's ratio, ranging from 364.15 to 405.90 N m^{-1} and from 0.32 to 0.34, respectively. Both PBE and HSE06 methods depict that all Janus $MSiGeN_4$ monolayers are indirect semiconductors with relatively large band gap values. The energy gaps are in the range from 1.48 (2.62) to 1.86 (2.97) eV using PBE (HSE06) functional. Besides, a small difference in work function on the different sides is found in all three Janus $MSiGeN_4$ monolayers due to their asymmetric atomic structures. The biaxial strain tunes the electronic band structure of all three monolayers $MSiGeN_4$ significantly. The band gaps are changed drastically, especially in the tensile strain case. In contrast, the effect of the electric fields on the electronic structures of the Janus $MSiGeN_4$ is weak. Our findings have enriched the group of septuple-atomic-layer materials and their potential for electronic applications.

Conflict of Interest

The authors declare no conflict of interest.

Data Availability Statement

The data that support the findings of this study are available from the corresponding author upon reasonable request.

Keywords

2D Janus structures, electronic properties, first-principles calculations

Received: July 12, 2022
Revised: August 18, 2022
Published online:

[1] K. S. Novoselov, A. K. Geim, S. V. Morozov, D. Jiang, Y. Zhang, S. V. Dubonos, I. V. Grigorieva, A. A. Firsov, *Science* **2004**, *306*, 666.
[2] N. A. Poklonski, S. A. Vyrko, A. I. Siahlo, O. N. Poklonskaya, S. V. Ratkevich, N. N. Hieu, A. A. Kocherzhenko, *Mater. Res. Express* **2019**, *6*, 042002.
[3] J. Li, L. Wang, J. Liu, R. Li, Z. Zhang, X.-Q. Chen, *Phys. Rev. B* **2020**, *101*, 081403(R).
[4] T.-N. Do, P.-H. Shih, H. Lin, D. Huang, G. Gumbs, T.-R. Chang, *Phys. Rev. B* **2022**, *105*, 235418.
[5] Q. H. Wang, K. Kalantar-Zadeh, A. Kis, J. N. Coleman, M. S. Strano, *Nat. Nanotechnol.* **2012**, *7*, 699.
[6] Q. Xiaofeng, L. Junwei, F. Liang, L. Ju, *Science* **2014**, *346*, 1344.
[7] C. V. Nguyen, N. N. Hieu, N. A. Poklonski, V. V. Ilyasov, L. Dinh, T. C. Phong, L. V. Tung, H. V. Phuc, *Phys. Rev. B* **2017**, *96*, 125411.
[8] N. N. Hieu, H. V. Phuc, V. V. Ilyasov, N. D. Chien, N. A. Poklonski, N. V. Hieu, C. V. Nguyen, *J. Appl. Phys.* **2017**, *122*, 104301.
[9] K. D. Pham, V. T. Vi, D. V. Thuan, N. V. Hieu, C. V. Nguyen, H. V. Phuc, B. D. Hoi, L. T. Phuong, N. Q. Cuong, D. V. Lu, N. N. Hieu, *Chem. Phys.* **2019**, *524*, 101.
[10] K. D. Pham, V. T. T. Vi, D. V. Thuan, L. T. T. Phuong, L. T. Hoa, N. V. Hieu, C. V. Nguyen, H. V. Phuc, H. R. Jappor, N. Q. Cuong, B. D. Hoi, N. N. Hieu, *Mater. Res. Express* **2019**, *6*, 115002.
[11] A. V. Lugovskoi, M. I. Katsnelson, A. N. Rudenko, *Phys. Rev. Lett.* **2019**, *123*, 176401.
[12] A.-Y. Lu, H. Zhu, J. Xiao, C.-P. Chuu, Y. Han, M.-H. Chiu, C.-C. Cheng, C.-W. Yang, K.-H. Wei, Y. Yang, Y. Wang, D. Sokaras, D. Nordlund, P. Yang, D. A. Muller, M.-Y. Chou, X. Zhang, L.-J. Li, *Nat. Nanotechnol.* **2017**, *12*, 744.
[13] J. Zhang, S. Jia, I. Kholmanov, L. Dong, D. Er, W. Chen, H. Guo, Z. Jin, V. B. Shenoy, L. Shi, J. Lou, *ACS Nano* **2017**, *11*, 8192.
[14] M. Yagmurcukardes, Y. Qin, S. Ozen, M. Sayyad, F. M. Peeters, S. Tongay, H. Sahin, *Appl. Phys. Rev.* **2020**, *7*, 011311.
[15] T. V. Vu, V. T. T. Vi, C. V. Nguyen, H. V. Phuc, N. N. Hieu, *J. Phys. D: Appl. Phys.* **2020**, *53*, 455302.
[16] T. V. Vu, V. T. T. Vi, H. V. Phuc, C. V. Nguyen, N. A. Poklonski, C. A. Duque, D. P. Rai, B. D. Hoi, N. N. Hieu, *J. Phys.: Condens. Matter* **2021**, *33*, 225503.
[17] T. V. Vu, V. T. T. Vi, H. V. Phuc, A. I. Kartamyshev, N. N. Hieu, *Phys. Rev. B* **2021**, *104*, 115410.
[18] H. T. T. Nguyen, V. T. T. Vi, T. V. Vu, N. V. Hieu, D. V. Lu, D. P. Rai, N. T. T. Binh, *RSC Adv.* **2020**, *10*, 44785.
[19] F. Li, W. Wei, P. Zhao, B. Huang, Y. Dai, *J. Phys. Chem. Lett.* **2017**, *8*, 5959.
[20] C. Yu, X. Cheng, C. Wang, Z. Wang, *Phys. E* **2019**, *110*, 148.
[21] Y. Guo, S. Zhou, Y. Bai, J. Zhao, *Appl. Phys. Lett.* **2017**, *110*, 163102.
[22] Y. Bai, Q. Zhang, N. Xu, K. Deng, E. Kan, *Appl. Surf. Sci.* **2019**, *478*, 522.
[23] W. Zhou, J. Chen, Z. Yang, J. Liu, F. Ouyang, *Phys. Rev. B* **2019**, *99*, 075160.
[24] Y.-L. Hong, Z. Liu, L. Wang, T. Zhou, W. Ma, C. Xu, S. Feng, L. Chen, M.-L. Chen, D.-M. Sun, X.-Q. Chen, H.-M. Cheng, W. Ren, *Science* **2020**, *369*, 670.
[25] L. Wang, Y. Shi, M. Liu, A. Zhang, Y.-L. Hong, R. Li, Q. Gao, M. Chen, W. Ren, H.-M. Cheng, Y. Li, X.-Q. Chen, *Nat. Commun.* **2021**, *12*, 2361.
[26] C. Q. Nguyen, Y. S. Ang, S.-T. Nguyen, N. V. Hoang, N. M. Hung, C. V. Nguyen, *Phys. Rev. B* **2022**, *105*, 045303.
[27] C. V. Nguyen, C. Q. Nguyen, S.-T. Nguyen, Y. S. Ang, N. V. Hieu, *J. Phys.Chem. Lett.* **2022**, *13*, 2576.
[28] Y. Yu, J. Zhou, Z. Guo, Z. Sun, *ACS Appl. Mater. Interfaces* **2021**, *13*, 28090.
[29] P. Giannozzi, S. Baroni, N. Bonini, M. Calandra, R. Car, C. Cavazzoni, D. Ceresoli, G. L. Chiarotti, M. Cococcioni, I. Dabo, A. D. Corso, S. de Gironcoli, S. Fabris, G. Fratesi, R. Gebauer, U. Gerstmann, C. Gougoussis, A. Kokalj, M. Lazzeri, L. Martin-Samos, N. Marzari, F. Mauri, R. Mazzarello, S. Paolini, A. Pasquarello, L. Paulatto, C. Sbraccia, S. Scandolo, G. Sclauzero, A. P. Seitsonen, et al., *J. Phys.: Condens. Matter* **2009**, *21*, 395502.
[30] J. P. Perdew, K. Burke, M. Ernzerhof, *Phys. Rev. Lett.* **1996**, *77*, 3865.
[31] J. Heyd, G. E. Scuseria, M. Ernzerhof, *J. Chem. Phys.* **2003**, *118*, 8207.

[32] S. Grimme, *J. Comput. Chem.* **2006**, *27*, 1787.
[33] T. Sohier, M. Calandra, F. Mauri, *Phys. Rev. B* **2017**, *96*, 075448.
[34] S. Ahmad, M. Idrees, F. Khan, C. Nguyen, I. Ahmad, B. Amin, *Chem. Phys. Lett.* **2021**, *776*, 138689.
[35] K.-A. N. Duerloo, M. T. Ong, E. J. Reed, *J. Phys. Chem. Lett.* **2012**, *3*, 2871.
[36] M. Born, K. Huang, *Am. J. Phys.* **1955**, *23*, 474.
[37] N. T. Hung, A. R. T. Nugraha, R. Saito, *J. Phys. D: Appl. Phys.* **2018**, *51*, 075306.
[38] P. Xiang, S. Sharma, Z. M. Wang, J. Wu, U. Schwingenschlögl, *ACS Appl. Mater. Interfaces* **2020**, *12*, 30731.
[39] S.-D. Guo, X.-S. Guo, R.-Y. Han, Y. Deng, *Phys. Chem. Chem. Phys.* **2019**, *21*, 24620.
[40] T. Cheng, H. Lang, Z. Li, Z. Liu, Z. Liu, *Phys. Chem. Chem. Phys.* **2017**, *19*, 23942.
[41] T. V. Vu, H. V. Phuc, S. Ahmad, V. Q. Nha, C. Van Lanh, D. P. Rai, A. I. Kartamyshev, K. D. Pham, L. C. Nhan, N. N. Hieu, *RSC Adv.* **2021**, *11*, 23280.
[42] C.-F. Fu, J. Sun, Q. Luo, X. Li, W. Hu, J. Yang, *Nano Lett.* **2018**, *18*, 6312.
[43] L. Bengtsson, *Phys. Rev. B* **1999**, *59*, 12301.
[44] H. Liu, Z. Huang, C. He, Y. Wu, L. Xue, C. Tang, X. Qi, J. Zhong, *J. Appl. Phys.* **2018**, *125*, 082516.
[45] D. Q. Khoa, D. T. Nguyen, C. V. Nguyen, V. T. Vi, H. V. Phuc, L. T. Phuong, B. D. Hoi, N. N. Hieu, *Chem. Phys.* **2019**, *516*, 213.
[46] T. V. Vu, C. V. Nguyen, H. V. Phuc, A. A. Lavrentyev, O. Y. Khyzhun, N. V. Hieu, M. M. Obeid, D. P. Rai, H. D. Tong, N. N. Hieu, *Phys. Rev. B* **2021**, *103*, 085422.
[47] L. Debbichi, O. Eriksson, S. Lebègue, *J. Phys. Chem. Lett.* **2015**, *6*, 3098.